Understanding glucose transport by the bacterial phosphoenolpyruvate. Glycose phosphotransferase system on the basis of kinetic measurements in vitro.

Rohwer, J.M.; Meadow, N.D.; Roseman, S.; Westerhoff, H.V.; Postema, P.

published in
Journal of Biological Chemistry
2000

DOI (link to publisher)
10.1074/jbc.M002461200

document version
Publisher's PDF, also known as Version of record

THE JOURNAL OF BIOLOGICAL CHEMISTRY
Vol. 275, No. 45, Issue of November 10, pp. 34909–34921, 2000

Printed in U.S.A.

Understanding Glucose Transport by the Bacterial Phosphoenolpyruvate:Glycose Phosphotransferase System on the Basis of Kinetic Measurements *in Vitro**

Received for publication, March 23, 2000, and in revised form, July 5, 2000
Published, JBC Papers in Press, July 10, 2000, DOI 10.1074/jbc.M002461200

Johann M. Rohwer‡§¶, Norman D. Meadow‖, Saul Roseman‖, Hans V. Westerhoff§, and Pieter W. Postma§**

*From the ‡Department of Biochemistry, University of Stellenbosch, Private Bag X1, 7602 Matieland, South Africa, the §E. C. Slater Institute, BioCentrum Amsterdam, University of Amsterdam, Plantage Muidergracht 12, NL-1018 TV Amsterdam, The Netherlands, the ‖Department of Biology, The Johns Hopkins University, Baltimore, Maryland 21218-2685, and the **Institute for Molecular Biological Sciences, BioCentrum Amsterdam, Vrije Universiteit, De Boelelaan 1087, NL-1081 HV Amsterdam, The Netherlands*

The kinetic parameters *in vitro* of the components of the phosphoenolpyruvate:glycose phosphotransferase system (PTS) in enteric bacteria were collected. To address the issue of whether the behavior *in vivo* of the PTS can be understood in terms of these enzyme kinetics, a detailed kinetic model was constructed. Each overall phosphotransfer reaction was separated into two elementary reactions, the first entailing association of the phosphoryl donor and acceptor into a complex and the second entailing dissociation of the complex into dephosphorylated donor and phosphorylated acceptor. Literature data on the K_m values and association constants of PTS proteins for their substrates, as well as equilibrium and rate constants for the overall phosphotransfer reactions, were related to the rate constants of the elementary steps in a set of equations; the rate constants could be calculated by solving these equations simultaneously. No kinetic parameters were fitted. As calculated by the model, the kinetic parameter values *in vitro* could describe experimental results *in vivo* when varying each of the PTS protein concentrations individually while keeping the other protein concentrations constant. Using the same kinetic constants, but adjusting the protein concentrations in the model to those present in cell-free extracts, the model could reproduce experiments *in vitro* analyzing the dependence of the flux on the total PTS protein concentration. For modeling conditions *in vivo* it was crucial that the PTS protein concentrations be implemented at their high *in vivo* values. The model suggests a new interpretation of results hitherto not understood; *in vivo*, the major fraction of the PTS proteins may exist as complexes with other PTS proteins or boundary metabolites, whereas *in vitro*, the fraction of complexed proteins is much smaller.

In many bacteria, the phosphoenolpyruvate:glycose phosphotransferase system (PTS)[1] is involved in the uptake and concomitant phosphorylation of a variety of carbohydrates (for reviews, see Refs. 1 and 2). The PTS is a group transfer pathway; a phosphoryl group derived from phosphoenolpyruvate (PEP) is transferred sequentially along a series of proteins to the carbohydrate molecule. The sequence of phosphotransfer is from PEP to the general cytoplasmic PTS proteins enzyme I (EI) and HPr and, in the case of glucose, further to the carbohydrate-specific cytoplasmic IIA^{Glc}, membrane-bound $IICB^{Glc}$ (the glucose permease), and glucose. For other carbohydrates, specific enzymes II exist (with the A, B, and C domains present either as a single polypeptide or as multiple proteins, depending on the carbohydrate that is transported), which accept the phosphoryl group from HPr (1–4).

Apart from its direct role in the above phosphotransfer and its indirect role in transport, IIA^{Glc} is an important signaling molecule, mediating catabolite repression (reviewed in Refs. 1, 2, and 5). The presence or absence of a PTS substrate affects the IIA^{Glc} phosphorylation state; in the absence of PTS substrate, phosphorylated IIA^{Glc} predominates, which activates adenylate cyclase and hence increases the intracellular cyclic AMP level, thereby affecting the expression of a large number of genes. The presence of a PTS substrate, on the other hand, will lead to dephosphorylation of IIA^{Glc}. Unphosphorylated IIA^{Glc} can bind stoichiometrically to the uptake systems for some non-PTS substrates for growth, inhibiting these uptake systems allosterically by so-called "inducer exclusion" and preventing the entry of the alternative carbon substrates into the cell to induce their own catabolic genes.

The individual components of the PTS have been characterized extensively, using kinetic and structural approaches (for a review, see Refs. 1, 2, 3, and 4). In the kinetic analysis of the PTS proteins, many K_m values for their substrates and products, as well as the equilibrium constants of the phosphotransfer reactions have been determined. A recent development is the direct determination, using a rapid quench method, of the forward and reverse rate constants of phosphotransfer between HPr and IIA^{Glc} of *Escherichia coli* (6).

Metabolic control analysis is a quantitative framework developed by Kacser and Burns (7) and Heinrich and Rapoport (8) for describing the steady-state behavior of metabolic systems and the dependence of cellular variables (*e.g.* fluxes or intermediate concentrations) on parameters (*e.g.* enzyme concentrations). The intracellular concentrations of all four glucose PTS

* This study was supported by the South African Foundation for Research Development, the Harry Crossley Foundation and the Netherlands Organization for Scientific Research. The costs of publication of this article were defrayed in part by the payment of page charges. This article must therefore be hereby marked "*advertisement*" in accordance with 18 U.S.C. Section 1734 solely to indicate this fact.

¶ To whom correspondence should be addressed: Dept. of Biochemistry, University of Stellenbosch, Private Bag X1, 7602 Matieland, South Africa. Tel.: 27 21 808 5843; Fax: 27 21 808 5863; E-mail: jr@maties.sun.ac.za.

[1] The abbreviations used are: PTS, phosphoenolpyruvate:glycose phosphotransferase system; PEP, phosphoenolpyruvate; EI, enzyme I; MeGlc, methyl α-D-glucopyranoside; PEG, polyethylene glycol.

proteins in *Salmonella typhimurium* (9) and of $IICB^{Glc}$ in *E. coli* (10) have been modulated in turn to determine the extent to which each of these proteins controls the PTS-mediated uptake rate *in vivo*. These dependences were quantified with so-called flux response coefficients, defined as the percentage change in the uptake rate upon a 1% increase in the enzyme concentration (see "Appendix" for mathematical definitions). Furthermore, titrations with different amounts of *E. coli* cell-free extracts (11) have enabled the quantification of the extent to which the glucose PTS proteins together control PTS-mediated phosphorylation activity *in vitro* at different protein concentrations. There was a remarkable difference between the results obtained *in vitro* and *in vivo*; *in vivo*, the four flux response coefficients added up to 0.8 (9), whereas *in vitro*, this sum varied between 1.5 and 1.8 depending on the total protein concentration (11). A value of greater than unity for this sum is in itself remarkable, since it reflects a higher order than linear dependence of flux on total protein concentration and contrasts strongly with the linear relationship between reaction rate and enzyme concentration usually found in enzyme kinetics. However, following these experiments, two additional questions are still unresolved. (*a*) What is the cause of the discrepancy between the sum of the flux response coefficients of the PTS proteins *in vivo* and *in vitro*, and why does this sum vary *in vitro* as the protein concentration changes? (*b*) Metabolic control analysis of group transfer pathways predicts that the sum of the enzyme flux response coefficients should lie between 1 and 2 (12). *In vivo*, this sum is less than 1; however, the flux response coefficients toward PEP, pyruvate, and glucose were not determined (9). Is it reasonable to assume that this sum increases to values above 1 if flux responses toward these "boundary metabolites" are included?

To address these questions and to determine whether such different behavior under conditions *in vivo* and *in vitro* may realistically be expected from the same metabolic system, we constructed a detailed kinetic model of the PTS in enteric bacteria, using literature data to assign values to the rate constants of the elementary phosphotransfer reactions. The results of steady-state calculations with the model are compared with experimental data, and the difference between experimental behavior of the PTS *in vivo* and *in vitro* is proposed to be the result of a novel aspect, *i.e.* the formation of long living transition state complexes between the different PTS proteins and the bound phosphoryl group.

The PTS may well be regarded as a paradigm for what has been termed "nonideal" metabolism (13). It is a group transfer pathway with special control properties (12); it is a perfect mechanistic example of metabolic channeling and therefore affected by macromolecular crowding (11); it is involved in signal transduction through catabolite repression and inducer exclusion (see above); and a similar sequence of phosphoryl transfer is ubiquitous in the "two-component regulatory systems" (14, 15), which have been proposed to form an intracellular "phosphoneural network" (16). Any attempt at a deeper understanding of such cellular processes at a level beyond map making, component identification, and characterization will have to put the pieces of the puzzle together in a quantitative "systems framework." This paper is such an attempt.

MATERIALS AND METHODS

Calculation of Rate Constants for Elementary Steps—A phosphotransfer reaction from a phosphoryl donor AP to an acceptor *E* can be symbolized as follows.

$$E + \mathrm{AP} \underset{k_{-\mathrm{I}}}{\overset{k_{\mathrm{I}}}{\rightleftharpoons}} E\mathrm{P} + \mathrm{A}$$

SCHEME 1

We shall use Roman numerals as subscripts to designate the rate constants for such an overall phosphotransfer reaction; the forward rate constant is k_{I}, and the reverse rate constant is $k_{-\mathrm{I}}$, yielding an equilibrium constant K_{eq} of $k_{\mathrm{I}}/k_{-\mathrm{I}}$. This overall reaction can be divided further into two elementary reactions, the first involving association of *E* and AP into the complex *E*PA, and the second involving dissociation of the complex into *E*P and A as follows.

$$E + \mathrm{AP} \underset{k_{-1}}{\overset{k_1}{\rightleftharpoons}} E\mathrm{PA} \underset{k_{-2}}{\overset{k_2}{\rightleftharpoons}} E\mathrm{P} + \mathrm{A}$$

SCHEME 2

Scheme 2 has four elementary rate constants, *i.e.* the forward and reverse rate constants of both the association and dissociation reactions, which will be denoted by subscripted arabic numerals. Scheme 2 is an extended description of Scheme 1, and in general the two will not be valid simultaneously. However, if the concentration of the intermediate complex *E*PA is assumed to be constant because its rate of production equals its rate of consumption (*i.e.* assuming a steady state for *E*PA), both reaction Schemes 1 and 2 are valid descriptions of the same process, and their rate constants can be related (see below).

We calculated the values of the rate constants for Scheme 2 from experimental data. Four types of data were available: (*a*) equilibrium constants for phosphotransfer reactions, (*b*) K_m values of some enzymes for their substrates or products, (*c*) association or dissociation equilibrium constants for some enzymes and substrates or products, and (*d*) rate constants of the type k_{I} and $k_{-\mathrm{I}}$ for the overall phosphotransfer reactions (Scheme 1).

First, the equilibrium constant was expressed as a function of the rate constants of the elementary steps as follows.

$$K_{\mathrm{eq}} = \frac{k_{\mathrm{I}}}{k_{-1}} = \frac{k_1 k_2}{k_{-1} k_{-2}} \qquad \text{(Eq. 1)}$$

Second, K_m values were related to the individual rate constants. Reaction Scheme 2 differs from that of a traditional enzyme in that the catalyst does not return unaltered. Only after *E*P has transferred its phosphoryl group to another molecule in additional reactions, free *E* is returned; also, the regeneration of AP requires additional reactions. Hence, the meaning of the Michaelis constant is also different. We applied the method analogous to that of Briggs-Haldane (17) by writing the differential equations and equating the time derivative of [*E*PA] to zero. This then allowed us to write rate equations for the zero product and the zero substrate case, which had the same form as the Michaelis-Menten equation. Hence, the K_m values of the "enzyme" *E* for AP and A (denoted with an asterisk to indicate this difference, *i.e.* $K^*_{m\mathrm{AP}}$ and $K^*_{m\mathrm{A}}$) are defined as follows.

$$K^*_{m\mathrm{AP}} = \frac{k_{-1} + k_2}{k_1} \qquad \text{(Eq. 2)}$$

and

$$K^*_{m\mathrm{A}} = \frac{k_{-1} + k_2}{k_{-2}} \qquad \text{(Eq. 3)}$$

The operational meaning of $K^*_{m\mathrm{AP}}$ is the concentration of AP giving half-maximal rates when both [*E*P] and [A] are negligible; that of $K^*_{m\mathrm{A}}$ is the concentration of A giving half-maximal reverse rates at zero [AP] and [*E*].

Third, association or dissociation equilibrium constants of enzymes and substrates or products were expressed in terms of rate constants of the elementary steps. Dissociation/association equilibrium constants of AP and A in Scheme 2 are given by the following.

$$K_{d\mathrm{AP}} = \frac{1}{K_{a\mathrm{AP}}} = \frac{k_{-1}}{k_1} \qquad \text{(Eq. 4)}$$

and

$$K_{d\mathrm{A}} = \frac{1}{K_{a\mathrm{A}}} = \frac{k_2}{k_{-2}} \qquad \text{(Eq. 5)}$$

It may be noted that the former K_a refers to the association to *E*, whereas the latter K_a refers to the association to *E*P.

Fourth, we related the rate constants of the overall phosphotransfer reactions (Scheme 1) to those where the complex was included explicitly

TABLE I
Parameters of the kinetic model

Parameters	Units	*In vivo*	*In vitro*	
			2 mg of protein/ml	6 mg of protein/ml
PTS protein concentrations				
$[EI]_{total}$	μM	5	0.04	0.12
$[HPr]_{total}$	μM	50	0.4	1.2
$[IIA^{Glc}]_{total}$	μM	40	0.32	0.96
$[IICB^{Glc}]_{total}$	μM	15	0.12	0.36
Boundary metabolite concentrations				
PEP	μM	2800	4000	12,000
Pyruvate	μM	900	0	0
MeGlc	μM	500	10,000	10,000
MeGlc 6-P	μM	50	0	0
Rate constants (PTS step in parentheses)				
k_1 (PEP to EI)	μM^{-1} min^{-1}		1960[a]	
k^{-1} (PEP to EI)	min^{-1}		480,000	
k_2 (PEP to EI)	min^{-1}		108,000	
k_{-2} (PEP to EI)	μM^{-1} min^{-1}		294	
k_3 (EI to HPr)	μM^{-1} min^{-1}		14,000	
k_{-3} (EI to HPr)	min^{-1}		14,000	
k_4 (EI to HPr)	min^{-1}		84,000	
k_{-4} (EI to HPr)	μM^{-1} min^{-1}		3360	
k_5 (HPr to IIA^{Glc})	μM^{-1} min^{-1}		21,960	
k_{-5} (HPr to IIA^{Glc})	min^{-1}		21,960	
k_6 (HPr to IIA^{Glc})	min^{-1}		4392	
k_{-6} (HPr to IIA^{Glc})	μM^{-1} min^{-1}		3384	
k_7 (IIA^{Glc} to $IICB^{Glc}$)	μM^{-1} min^{-1}		880	
k_{-7} (IIA^{Glc} to $IICB^{Glc}$)	min^{-1}		880	
k_8 (IIA^{Glc} to $IICB^{Glc}$)	min^{-1}		2640	
k_{-8} (IIA^{Glc} to $IICB^{Glc}$)	μM^{-1} min^{-1}		960	
k_9 ($IICB^{Glc}$ to Glc)	μM^{-1} min^{-1}		260	
k_{-9} ($IICB^{Glc}$ to Glc)	min^{-1}		389	
k_{10} ($IICB^{Glc}$ to Glc)	min^{-1}		4800	
k_{-10} ($IICB^{Glc}$ to Glc)	μM^{-1} min^{-1}		5.4×10^{-3}	

[a] Identical values were used for the rate constants under all conditions.

(Scheme 2). By following a steady-state treatment (18) for the complex *E*PA, one can derive the following.

$$k_I = \frac{k_1 k_2}{k_{-1} + k_2} \quad \text{(Eq. 6)}$$

and

$$k_{-I} = \frac{k_{-1} k_{-2}}{k_{-1} + k_2} \quad \text{(Eq. 7)}$$

Using the approaches outlined in Equations 1–7, a set of four independent equations was generated for each phosphotransfer reaction of the PTS, relating the kinetic parameters K_m^*, K_d, K_a, K_{eq}, k_I, and k_{-I} to the elementary rate constants. The equations were solved simultaneously for the rate constants of the elementary steps on the basis of experimental values of the kinetic parameters. The derivations of the elementary rate constants for the five phosphotransfer reactions of the glucose PTS are given under "Appendix."

Reaction Scheme 2 may be divided further by including the step $E \cdot PA \rightleftharpoons EP \cdot A$ explicitly, yielding three elementary steps in total. However, we did not consider this case, since insufficient data were available to assign values to all the rate constants in such a mechanism.

Model Parameters—To simulate the reactions of the PTS numerically, a few parameters other than the rate constants of the elementary reactions are required: the total concentration of each PTS protein and the concentrations of the boundary metabolites PEP, pyruvate, glucose (or methyl α-D-glucopyranoside (MeGlc), its nonmetabolizable analogue), and glucose 6-phosphate (or MeGlc 6-phosphate). The subunit molecular masses of the cytoplasmic PTS proteins EI (63,489), HPr (9109), and IIA^{Glc} (18,099) (19) were used to calculate intracellular concentrations of 5 μM (EI monomers), 20–100 μM (HPr), and 20–60 μM (IIA^{Glc}) from the intracellular amounts of these proteins reported in the literature (20–23). An intracellular volume of 2.5 μl/mg dry mass (24–26) was assumed in the calculations. Because $IICB^{Glc}$ is a membrane protein, intracellular amounts were reported on the activity level. Intracellular $IICB^{Glc}$ amounted to 10 μmol/liter cytoplasmic volume, as calculated from the specific activity of the protein and the glucose phosphorylation activity of *E. coli* given in Ref. 27.

For *E. coli* growing exponentially on glucose, intracellular PEP levels of 60–300 μM (28, 29) and pyruvate levels of 0.36–8 mM (28, 30) have been reported. These PEP values may underestimate the intracellular concentration, due to the long filtration time (up to 60 s) employed by the authors for sampling (see discussion in Ref. 31). Furthermore, transport assays in our laboratory are routinely performed with washed, concentrated, and starved cell suspensions (32). Under these conditions, intracellular PEP and pyruvate levels have recently been determined for glucose-grown *E. coli*; the PEP concentration was 2.8 mM, and that of pyruvate was 0.9 mM (33). We used these values for our simulations of PTS uptake assays. The MeGlc concentration was set to 500 μM, a concentration used routinely for uptake assays. Intracellular MeGlc 6-phosphate was fixed at 50 μM. During PTS-mediated carbohydrate uptake, intracellular carbohydrate phosphates will accumulate, their concentrations increasing from initial values close to zero when the substrate is a nonmetabolizable analogue. Numerical simulation of the PTS requires, however, that the boundary metabolite concentrations be fixed; otherwise, calculation of a steady state will be impossible. The chosen low MeGlc 6-phosphate concentration reflects the situation during the initial stages of the uptake process; in addition, we verified that increasing this value to 6 mM had negligible effect (less than 0.1%) on the observed flux (at 6 mM Glc·P, the dissociation of $IICB^{Glc} \cdot P \cdot Glc$ into $IICB^{Glc}$ and Glc · P should be >99% irreversible; *cf.* "Appendix").

When simulating PTS-mediated phosphorylation *in vitro*, the rate constants of the elementary steps were left unchanged. The dilution of the cytoplasmic proteins in our cell-free extracts in comparison to the intracellular environment was accounted for by calculating a dilution factor from the protein concentration of our extract and the reported intracellular total protein concentration of 0.25 g/ml (34). The intracellular concentrations of the PTS proteins were multiplied by this dilution factor to calculate their concentrations in the cell extract. Concentrations of the boundary substrates PEP, pyruvate, MeGlc, and MeGlc 6-phosphate were entered as employed under the experimental conditions.

All parameter values of the kinetic model are summarized in Table I. Concentrations of the PTS proteins and of the boundary metabolites are shown for the simulation of PTS activity *in vivo* and at two protein concentrations *in vitro*.

Numerical Methods—Simulations and steady-state calculations of the kinetic models were performed on an IBM-compatible personal

TABLE II

Steady-state properties of the kinetic model and comparison with experimental values

The flux J, the flux response coefficients of the four glucose PTS proteins, and their sum R^J_{PTS} were calculated with the parameter set of Table I for conditions *in vivo* and *in vitro* at two protein concentrations. R^J_{IIA} and R^J_{IICB} refer to the flux response coefficients with respect to the total concentrations of IIA^{Glc} and $IICB^{Glc}$, respectively.

Steady-state variable	*In vivo*		*In vitro*			
			2 mg of protein/ml		6 mg of protein/ml	
	Model	Experiment[a]	Model	Experiment[b]	Model	Experiment[b]
J (μM min^{-1})	1.4×10^4	2.2×10^4	13	18	97	144
R^J_{EI}	0.05	0	0.07	ND[c]	0.07	ND
R^J_{HPr}	−0.02	≤0.01	0.08	ND	0.05	ND
R^J_{IIA}	0.2	≤0.02	0.9	ND	0.7	ND
R^J_{IICB}	0.9	0.7	0.9	ND	0.9	ND
R^J_{PTS}	1.1	0.7–0.8	1.9	2.0	1.7	1.7

[a] Experimental data from Ref. 9.

[b] Experiments performed as in Ref. 11, except that glucose was used as carbon source for the cultivation of *E. coli* PJ4004.

[c] ND, not determined.

computer with the metabolic modeling program SCAMP (35). The calculations were checked with Gepasi (36).

Parameter Sensitivity Analysis—To determine the sensitivity of the kinetic model to the choices made for the kinetic parameters, we calculated the flux response coefficients with respect to those parameters (for details see "Appendix"). The flux response coefficient of a parameter was a measure of the sensitivity of the steady-state flux to changes in that specific parameter.

RESULTS

Here, we shall describe the kinetic behavior of the model and compare this to experimental results obtained *in vivo* and *in vitro*. Furthermore, a parameter sensitivity analysis will be presented to determine to what extent the results depended on assumptions that were made during the derivation of the rate constants of the elementary steps from the phenomenological kinetic constants measured experimentally (see "Appendix").

Steady-state Behavior—The steady-state flux predicted by the enzyme kinetic parameters of the PTS is shown in Table II for simulation of a PTS uptake assay *in vivo* and a phosphorylation experiment *in vitro* at two different protein concentrations. The corresponding experimental values are for comparison. For the modeled flux, agreement between model and experiment was good; although the modeled value was always lower than the experimental value, the discrepancy was only approximately 30% (*i.e.* less than a factor of 2) for conditions *in vivo* and *in vitro*. This discrepancy is small considering the fact that the calculation was based exclusively on experimentally determined parameters; no parameter value was fitted.

Next, we investigated whether the model would match experimental data obtained by varying the concentrations of the PTS proteins. The effect of changing in turn the concentrations of EI, HPr, IIA^{Glc}, and $IICB^{Glc}$ on PTS uptake activity (while keeping enzyme concentrations other than the modulated one constant) has been determined experimentally (9); these experiments were mimicked by numerical simulation. First we considered small variations, expressing the results in terms of response coefficients (*i.e.* the percentage change in flux for a 1% increase in enzyme concentration). Table II shows that the calculated response coefficients matched their experimental counterparts remarkably well.

A reservation concerning the use of response coefficients is that they refer to small parameter changes, whereas in biologically relevant cases, changes may well exceed 50%. We therefore also considered large variations in enzyme concentrations. Again the simulation results agreed remarkably well with experimental data: the modeled flux *versus* PTS protein concentration profiles matched the experimental ones (Fig. 1). An exception was the decrease in PTS uptake activity for high EI levels (9), which was not observed in the simulations. Fig. 1 also shows that changing the concentrations of EI, HPr, and IIA^{Glc} around their wild-type levels had little effect on the flux; this was quantified by calculating the flux response coefficients of these proteins, as indicated on the graphs. The flux response coefficients of IIA^{Glc} and $IICB^{Glc}$ were slightly higher than the experimentally reported values (*cf.* Table II).

A kinetic model will gain credibility if it can describe experimental data *in vivo* as well as *in vitro* without the need for adjustment of the kinetic parameters. The effect of concomitant changes in the concentrations of all proteins of the glucose PTS on its phosphorylation activity *in vitro* has been investigated experimentally by performing a PTS activity assay with different amounts of cell extract (11). We mimicked these experiments by numerical simulation (Fig. 2). As was observed experimentally (Figs. 1 and 2 in Ref. 11), the dependence of the flux on total protein concentration was more than linear but less than quadratic (Fig. 2*a*). Accordingly, the combined PTS flux response coefficient (R^J_{PTS}) decreased from almost 2 to around 1.7 as the protein concentration was increased from low values to 6 mg/ml (Fig. 2*b*).

In previous experiments, the macromolecular crowding agent PEG 6000 (37, 38) has been added to a PTS activity assay to mimic high intracellular macromolecule concentrations, and its effect was simulated with a simple kinetic model (11). We now proceeded to model macromolecular crowding with the complete model of the PTS by following a similar approach as in Ref. 11; the addition of PEG 6000 to the assay mixture was assumed to increase the on-rate constants for complex formation between the proteins and decrease the off-rate constants for complex dissociation by the same factor, α. Comparing Fig. 2 with Fig. 1, *a* and *b*, in Ref. 11, we see that the model agreed well with the experimental results; the addition of 9% PEG 6000 (simulated by $\alpha = 7$) stimulated the flux slightly at low protein concentrations and inhibited the flux at higher protein concentrations. A lower concentration (4.5%) of PEG 6000 (simulated by $\alpha = 4$) stimulated the flux over the whole range of protein concentrations. As was the case with PEG 6000 addition experimentally, the combined flux response coefficient R^J_{PTS} decreased more sharply in the model when the parameter α was increased (Fig. 2*b*); the decrease was sharper for 9% PEG 6000 and $\alpha = 7$ than for 4.5% PEG 6000 and $\alpha = 4$.

Metabolic control analysis of group transfer pathways has provided us with an analytical proof that the sum of the flux response coefficients of the proteins in a group transfer pathway can range from below 1 to 2 (12) and that values closer to 1 can result from increased complex formation between the proteins or a protein and a boundary metabolite. The absence of these complexes, on the other hand, leads to a value of 2 for this sum (39). As has been pointed out under "Discussion" of Ref. 11, decreasing R^J_{PTS} values with increasing protein concentration

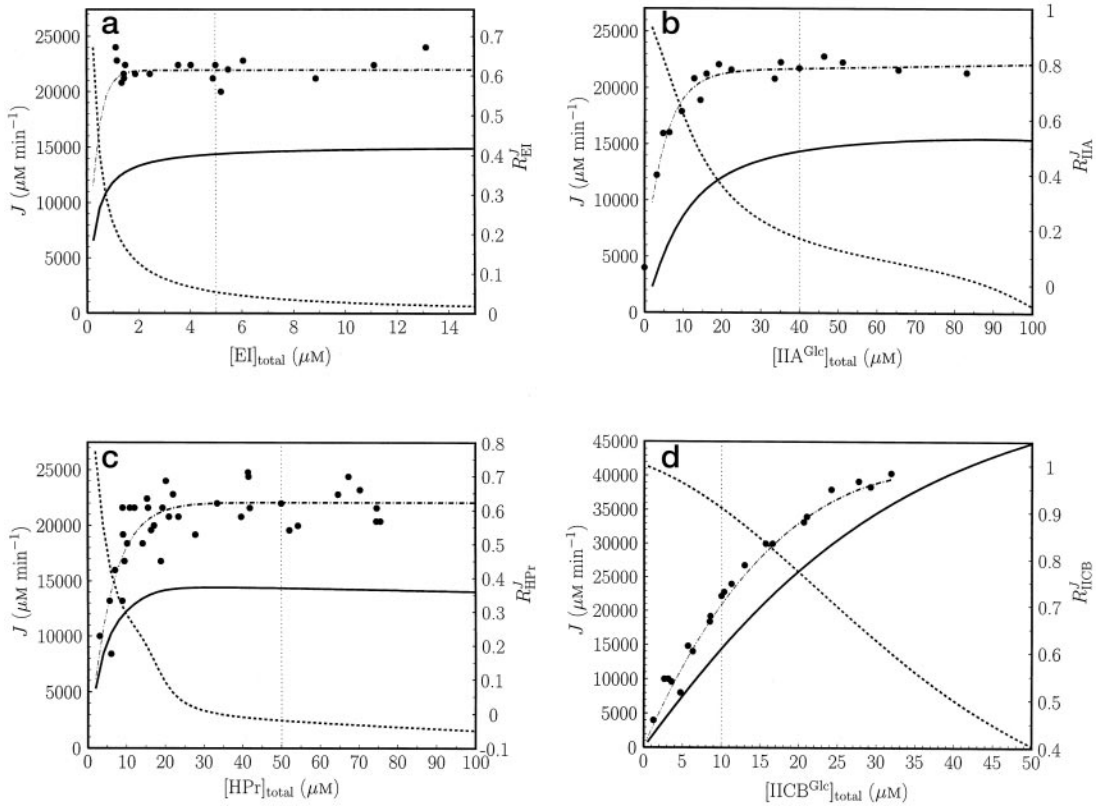

FIG. 1. **Dependence of the calculated PTS flux *in vivo* on the concentrations of the PTS proteins EI, HPr, IIA$^{\rm Glc}$, and IICB$^{\rm Glc}$.** Simulations were performed with the kinetic parameters *in vivo* of Table I. The concentration of each PTS protein was modulated in turn over the indicated range while keeping the other concentrations at their reference (wild-type) values. This mimics the experiments performed by van der Vlag and co-workers (Fig. 6 in Ref. 9); these data are included in the figure for reference. Wild-type levels are shown by *vertical dotted lines*. The modeled flux J is indicated by a *solid line* and shown on the *left y axis*; the modeled flux response coefficient of the respective protein is indicated by a *dotted line* and shown on the *right y axis*. Experimental flux data (9) are indicated by *solid circles* (raw data) and *dashed-dotted lines* (fitted curves from the original paper). EI (*a*), HPr (*b*), IIA$^{\rm Glc}$ (*c*), and IICB$^{\rm Glc}$ (*d*) concentration profiles are shown.

suggest increased complex formation between the proteins of the PTS. We investigated this point further by calculating with the kinetic model, using parameter values simulating *in vivo* and values simulating *in vitro* at protein concentrations of 2 and 6 mg/ml (Table I), the fraction of the different PTS proteins that was free (uncomplexed) and the fraction that was complexed with other proteins or boundary metabolites (Table III). For each condition, the concentrations of all the species and their relative proportions are indicated. The kinetic parameters implied that the major fraction of the PTS proteins should exist in the complexed state *in vivo* (Table III). This was in accordance with the $R^J_{\rm PTS}$ value close to 1 (Table II). Simulating conditions *in vitro* showed that the fraction of the proteins that existed in the complexed state was much lower but increased significantly with an increase in the protein concentration from 2 to 6 mg/ml. We also verified that increasing the parameter α to mimic macromolecular crowding caused a further increase in the fraction of PTS proteins existing in the complexed state (data not shown).

Parameter Sensitivity Analysis—Of course, the kinetic parameters used in the derivation of the rate constants (see "Appendix") were subject to experimental variability. In addition, insufficient data were available in some cases to calculate the rate constants from the kinetic parameters, and assumptions had to be made (*e.g.* Equation 21). To establish how strongly the behavior of the model depended on the choices for the kinetic parameters, the sensitivity of the steady-state flux under conditions *in vivo* to changes in these parameters was calculated as outlined under "Appendix." The sensitivity of the calculated flux to an uncertainty in a parameter value is quantified by the corresponding response coefficient.

The flux response coefficients of all model parameters (when simulating conditions *in vivo*) are listed in Table IV. In general, the flux response coefficients were small, indicating that the calculated flux did not depend crucially on the absolute magnitude of the chosen parameters, also when the reported literature values varied over a considerable range (*e.g.* $K_{m\rm PEP}$ or $K^*_{m\rm HPr}$). Notably, the parameters, the values of which had to be assumed altogether to solve for the rate constants of phosphotransfer reactions II–IV ($K_{a\rm II}$, $K_{a\rm III}$, and $K_{a\rm IV}$), had low flux response coefficients, which precludes any unusually large uncertainty in the calculated flux. The only parameters with large flux response coefficients were $K^*_{m\rm IIAGlc\text{-}P}$, $k_{\rm IV}$, $K_{m\rm Glc}$, $k_{\rm V}$, and $[{\rm IICB^{Glc}}]_{\rm total}$ (0.5, 0.7, 0.3, 0.3, and 0.9, respectively). This was not entirely unexpected for the following reasons. First, modulations in both $K^*_{m\rm IIAGlc\text{-}P}$ and $k_{\rm IV}$ resulted in an equal relative change in the rate constant k_8 (Equation 40), and the flux control coefficient of reaction 8 (*i.e.* from IIA$^{\rm Glc}$ · P · IICB$^{\rm Glc}$ to IIA$^{\rm Glc}$ and IICB$^{\rm Glc}$ · P) in the model was high ($C^J_8 = 0.6$); second, modulations in both $K_{m\rm Glc}$ and $k_{\rm V}$ resulted in an equal relative change in the rate constant k_{10} (Equation 48), and the flux control coefficient of reaction 10 (*i.e.* from IICB$^{\rm Glc}$ · P · Glc to IICB$^{\rm Glc}$ and Glc · P) in the model was relatively high ($C^J_{10} = 0.3$); third, as shown by theory (12), both a high C^J_8 and a high C^J_{10} are consistent with a high $R^J_{\rm IICB}$; and finally, IICB$^{\rm Glc}$ was the only PTS protein in the model with a high flux response coefficient, in agreement with experimental results (9, 10).

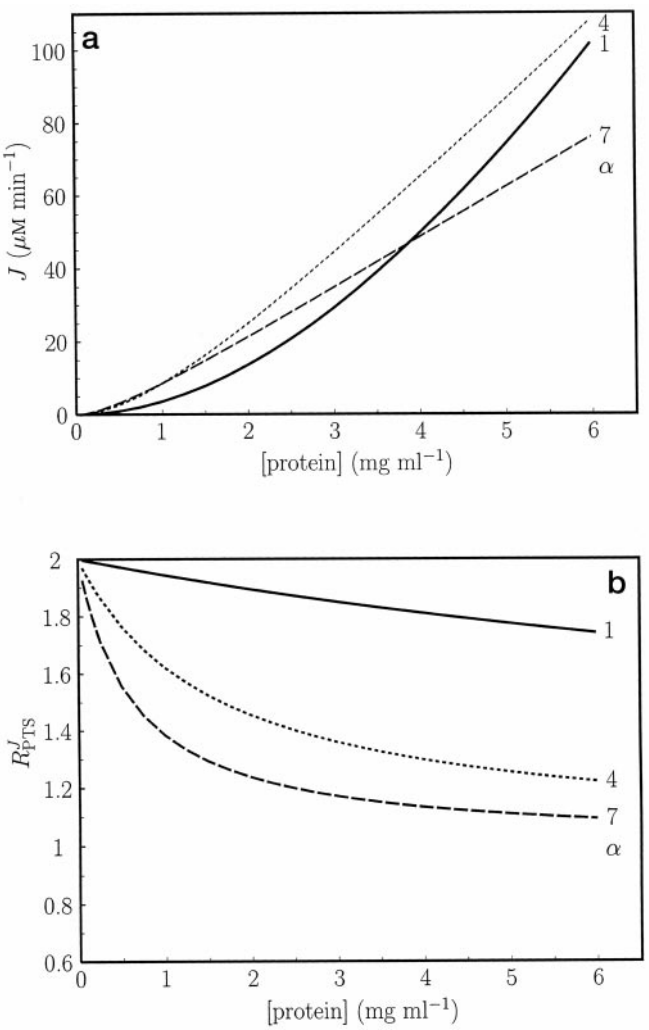

FIG. 2. **Dependence of the calculated PTS flux *in vitro* on the total protein concentration when increasing all PTS proteins and PEP together.** Simulations were performed with the kinetic parameters *in vitro* of Table I. The concentrations of the PTS proteins for a certain protein concentration were calculated by assuming a total intracellular protein concentration of 0.25 g/ml, as described under "Materials and Methods." The concentration of PEP in mM was set to twice the protein concentration in mg/ml, corresponding to the experiments in Ref. 11. The addition of the macromolecular crowding agent PEG 6000 to the assay mixture was simulated by increasing the rate constants that lead to complex formation between proteins by a factor α and decreasing the rate constants of protein-protein complex dissociation by the same factor α (see also Ref. 11). The rate constants for interactions between a protein and a boundary metabolite were left unchanged. Thus, k_3, k_{-4}, k_7, and k_{-8} were multiplied by α, and k_{-3}, k_4, k_{-7}, and k_8 were divided by α. The flux J (*a*) and the combined flux response coefficient of EI, HPr, IIA^{Glc}, and $IICB^{Glc}$ (R^J_{PTS}) (*b*) are shown as a function of protein concentration for α = 1, 4, and 7.

DISCUSSION

Experimental metabolic control analysis of the glucose PTS *in vivo* (9, 10) and *in vitro* (11) has yielded many interesting experimental results and increased our understanding of this group transfer pathway in particular and of other information transfer pathways such as the two-component regulatory systems (15, 16) in general. For example, $IICB^{Glc}$ was the only PTS protein that controlled MeGlc uptake *in vivo* to any significant extent (9, 10), and the combined flux response coefficient of the glucose PTS proteins *in vitro* was higher than *in vivo* and moreover depended on the protein concentration in the assay, suggesting that substantial complex formation between the PTS proteins may occur *in vivo* (11).

This paper reports on the construction of a detailed kinetic model of the PTS. The model can describe experimental data and suggests a new interpretation of results that have not yet been explained fully, as we shall discuss below. There was good agreement between model and experiment *in vivo*, both for flux values and flux response coefficients (Table II). Furthermore, the same model parameters could simulate conditions *in vitro* (Table II, Fig. 2). The fact that experimental and simulated R^J_{PTS} values agreed well (Table II) indicates that the degree of complex formation between the PTS proteins *in vitro* was modeled correctly. Furthermore, the model shows that the combined PTS flux response coefficient (and hence, the degree of complex formation between the proteins) can differ markedly between conditions *in vivo* and *in vitro*.

Prior to this study, two questions brought up by experimental results were still unresolved: first, the discrepancy between the combined flux response coefficient of the four glucose PTS proteins *in vivo* (9) and *in vitro* (11) had yet to be explained fully; second, the combined flux response coefficient of 0.8 for the four glucose PTS proteins *in vivo* (9) was less than unity, while theory predicts a value between 1 and 2 when including flux responses to the boundary metabolites (12).

Both of these issues have essentially been resolved in this paper. First, the model could calculate different values of R^J_{PTS} with the *same* model parameters, depending on whether conditions *in vivo* or *in vitro* were simulated. The difference stems from the higher degree of complex formation between the PTS proteins *in vivo* (Table III). Regarding the second issue, a value of 1.5 was previously derived for R^J_{PTS} when including the boundary metabolites on the grounds that R^J_{MeGlc} equaled R^J_{IICB} (9), which would fit with the theoretical prediction. However, an equality between R^J_{IICB} and R^J_{MeGlc} only holds if no complexes exist between the different PTS proteins or between a protein and a boundary metabolite (12). Both the present modeling results (Table III) and the experimental determination of R^J_{PTS} *in vitro* (11) argue against this assumption, as they suggest that complex formation between the PTS proteins plays an important role *in vivo*. Nevertheless, the boundary metabolites could in principle account for the difference between 0.8 and 1 and increase the combined response coefficient to values between 1 and 2. Our model, however, does not support this explanation, since R^J_{PEP}, R^J_{Pyr}, R^J_{MeGlc}, and R^J_{MeGlcP} were low when simulating *in vivo* conditions (Table IV). A possible reason for a decrease in R^J_{PTS} to values below 1 is the formation of abortive, noncatalytic complexes between two or more proteins. For example, IIA^{Glc} has been shown to bind HPr when both proteins are unphosphorylated (40). Such abortive complexes were not taken into account in the kinetic model for lack of detailed knowledge concerning the relevant equilibrium binding constants.

In constructing the kinetic model, we used kinetic parameters for glucose and not for MeGlc (its nonmetabolizable analogue), although MeGlc was used for both the uptake experiments *in vivo* (9) and the flux analyses *in vitro* (11). The reasons for this were 2-fold. First, there was a large discrepancy between reported K_m values for MeGlc (170 μM *in vivo* and 6 μM *in vitro*) whereas the K_m values for glucose agreed much better (20 μM *in vivo* and 10 μM *in vitro*) (41). Second, the K_d value, which was used in the calculations (Equation 43), had only been determined for glucose (42). The agreement between model and experiment, also for large ranges of parameter variation (Figs. 1 and 2), suggests that selecting the parameters for glucose (and not for MeGlc) was not crucial in the present analysis.

The agreement between model and experiment is even more significant when one considers that the present model is based

TABLE III
Simulated distribution of PTS protein species under different conditions
Steady-state calculations were performed with the parameters of Table I for conditions *in vivo* and two protein concentrations *in vitro*.

Species	*In vivo*		*In vitro*			
			2 mg of protein/ml		6 mg of protein/ml	
	Concentration	Percentage of total	Concentration	Percentage of total	Concentration	Percentage of total
	μM	%	nM	%	nM	%
EI species						
EI · P · Pyr	3.1	61.0	0.12	0.3	0.9	0.7
EI	0.27	5.4	0.01	0.02	0.02	0.02
EI · P	1.2	23.8	39.7	99.3	118	98.3
EI · P · HPr	0.49	9.8	0.16	0.4	1.2	1.0
Total EI	5.0	100	40	100	120	100
HPr species						
EI · P · HPr	0.5	1.0	0.2	0.04	1	0.1
HPr	1.3	2.6	27	6.8	67	5.5
HPr · P	30	59.6	364	90.9	1069	89.1
HPr · P · IIA^{Glc}	18	36.9	9	2.2	63	5.2
Total HPr	50	100	400	100	1200	100
IIA^{Glc} species						
HPr · P · IIA^{Glc}	18	46.2	9	2.8	63	6.6
IIA^{Glc}	0.6	1.6	26	8.2	63	6.6
IIA^{Glc} · P	15	38.5	280	87.4	798	83.1
IIA^{Glc} · P · $IICB^{Glc}$	5.5	13.7	5	1.6	37	3.8
Total IIA^{Glc}	40	100	320	100	960	100
$IICB^{Glc}$ species						
IIA^{Glc} · P · $IICB^{Glc}$	5.5	54.7	5.1	6.3	37	15.2
$IICB^{Glc}$	1.4	14.1	72	90.2	183	76.4
$IICB^{Glc}$ · P	0.1	1.2	0.01	0.01	0.04	0.02
$IICB^{Glc}$ · P · MeGlc	3.0	29.9	2.8	3.5	20	8.4
Total $IICB^{Glc}$	10	100	80	100	240	100
Proteins in complexes		63		4		10
Proteins uncomplexed		37		96		90

directly on kinetic data. Experimentally determined parameters taken from the literature were entered in the model; they were not subject to a fitting procedure. The flux calculated with the model was generally insensitive to changes in the kinetic parameters that were used in the derivation of the kinetic rate constants (Table IV), indicating that our selection of a parameter from a range of literature values, or the assumption of a value where no data were available, did not bias the result significantly. The high parameter sensitivities toward $K^*_{mIIAGlc\text{-}P}$ and k_{IV} (and hence to k_8) as well as to K_{mGlc} and k_V (and hence to k_{10}) were in agreement with the suggestion (9), based on the determination of R^J_{IICB} *in vivo*, that the flux control coefficients of the fourth and fifth phosphotransfer reactions (from phosphorylated IIA^{Glc} to glucose or MeGlc) *in vivo* are high.

In the construction of the model, we have made some simplifications. First, we did not take into account that EI can dimerize. The dimer is the active form (43–45); the monomer-dimer equilibrium depends on PEP, Mg(II) ions, and temperature, and phosphorylation shifts the equilibrium significantly to the monomeric state (46, 47). Detailed studies of the monomer-dimer transition (46, 48, 49) have also shown that the monomer cannot be phosphorylated by PEP, leading to a model proposing that an active EI dimer is phosphorylated by PEP and then dissociates into two phosphorylated monomers, which subsequently pass the phosphoryl group to HPr and redimerize (1, 50, 51). This cycle was not included in the present kinetic model, since insufficient data were available on the additional rate constants involved. Moreover, at EI concentrations present *in vivo*, it should be virtually only dimer. Since there is no suggestion of cooperativity of the two subunits during phosphorylation, we conclude that it is valid to treat EI as a monomer for the kinetic equations presented in this paper.

Second, $IICB^{Glc}$, the membrane-bound glucose permease, has also been shown to exist in dimeric form (52, 53), and immunoprecipitation experiments have suggested that four IIA^{Glc} molecules are bound to the $IICB^{Glc}$ dimer (53). We have not included this phenomenon in the kinetic model either for lack of kinetic details.

Third, the kinetic model ignores the vectorial nature and compartmentation of the uptake process. The reactions are simulated as if they occurred in a well stirred reactor; however, PTS-mediated uptake entails that extracellular glucose or MeGlc be taken up and phosphorylated to yield intracellular glucose 6-phosphate or MeGlc 6-phosphate. For modeling purposes, this should have no consequences, since there are no extracellular pools of variable metabolites. The extracellular glucose (or MeGlc) concentration is a fixed parameter, as is the intracellular glucose 6-phosphate (MeGlc 6-phosphate) concentration; it was not required, therefore, to enter the different volumes of the extracellular and intracellular compartments in the model.

A final simplification concerns the organism described. Most of the kinetic data used in the model are from *E. coli*, while the physiological uptake experiments with varying PTS protein levels were performed on *S. typhimurium*. Because of the identity of HPr and near identity of EI and IIA^{Glc} in the two organisms (2), this should pose no problem. Even the $IICB^{Glc}$ proteins from both organisms have very similar kinetic properties despite differences in their isoelectric points and specific activities (27). In addition, variation of intracellular $IICB^{Glc}$ levels in *E. coli* and *S. typhimurium* leads to very similar physiological responses (9, 10). We have therefore combined as much as possible of the available data on both organisms into a general model of the glucose PTS in enteric bacteria.

Calculations with the kinetic model show that under conditions *in vivo* the largest proportion of the PTS exists as long living transition state complexes, either between two PTS proteins and the bound phosphoryl group or between a protein, a boundary substrate, and the bound phosphoryl group (Table III). In contrast, under conditions *in vitro* a much larger frac-

TABLE IV
Parameter sensitivity analysis of the kinetic model

Parameter p	PTS step	Equation[a]	Units	Reference value	$R_p^{J\,b}$
$K_{m\mathrm{PEP}}$	PEP to EI	10	μM	300	3×10^{-2}
$K_{m\mathrm{Pyr}}$	PEP to EI	11	μM	2000	6×10^{-3}
K_{eqI}	PEP to EI	12	Dimensionless	1.5	4×10^{-2}
k_{I}	PEP to EI	13	$\mu\mathrm{M}^{-1}$ min^{-1}	360	2×10^{-3}
$K^*_{m\mathrm{HPr}}$	EI to HPr	18	μM	7	2×10^{-3}
k_{II}	EI to HPr	19	$\mu\mathrm{M}^{-1}$ min^{-1}	12,000	7×10^{-2}
$k_{-\mathrm{II}}$	EI to HPr	20	$\mu\mathrm{M}^{-1}$ min^{-1}	480	-2×10^{-2}
$K_{a\mathrm{II}}$	EI to HPr	21	$\mu\mathrm{M}^{-1}$	1	-3×10^{-3}
$K^*_{m\mathrm{HPr}\cdot\mathrm{P}}$	HPr to IIA$^{\mathrm{Glc}}$	26	μM	1.2	1×10^{-2}
k_{III}	HPr to IIA$^{\mathrm{Glc}}$	27	$\mu\mathrm{M}^{-1}$ min^{-1}	3,660	8×10^{-2}
$k_{-\mathrm{III}}$	HPr to IIA$^{\mathrm{Glc}}$	28	$\mu\mathrm{M}^{-1}$ min^{-1}	2,820	-6×10^{-2}
$K_{a\mathrm{III}}$	HPr to IIA$^{\mathrm{Glc}}$	29	$\mu\mathrm{M}^{-1}$	1	-6×10^{-2}
$K^*_{m\mathrm{IIAGlc}\cdot\mathrm{P}}$	IIA$^{\mathrm{Glc}}$ to IICB$^{\mathrm{Glc}}$	34	μM	4	5×10^{-1}
k_{IV}	IIA$^{\mathrm{Glc}}$ to IICB$^{\mathrm{Glc}}$	35	$\mu\mathrm{M}^{-1}$ min^{-1}	660	7×10^{-1}
$k_{-\mathrm{IV}}$	IIA$^{\mathrm{Glc}}$ to IICB$^{\mathrm{Glc}}$	36	$\mu\mathrm{M}^{-1}$ min^{-1}	240	-3×10^{-3}
$K_{a\mathrm{IV}}$	IIA$^{\mathrm{Glc}}$ to IICB$^{\mathrm{Glc}}$	37	$\mu\mathrm{M}^{-1}$	1	-3×10^{-3}
$K_{m\mathrm{Glc}}$	IICB$^{\mathrm{Glc}}$ to Glc	42	μM	20	3×10^{-1}
$K_{d\mathrm{Glc}}$	IICB$^{\mathrm{Glc}}$ to Glc	43	μM	1.5	4×10^{-6}
K_{eqV}	IICB$^{\mathrm{Glc}}$ to Glc	44	Dimensionless	5.9×10^5	7×10^{-6}
k_{V}	IICB$^{\mathrm{Glc}}$ to Glc	45	$\mu\mathrm{M}^{-1}$ min^{-1}	240	3×10^{-1}
$[\mathrm{EI}]_{\mathrm{total}}$			μM	5	5×10^{-2}
$[\mathrm{HPr}]_{\mathrm{total}}$			μM	50	-2×10^{-2}
$[\mathrm{IIA^{Glc}}]_{\mathrm{total}}$			μM	40	2×10^{-1}
$[\mathrm{IICB^{Glc}}]_{\mathrm{total}}$			μM	10	9×10^{-1}
[PEP]			μM	2800	2×10^{-2}
[Pyruvate]			μM	900	-5×10^{-2}
[MeGlc]			μM	500	1×10^{-2}
[MeGlc 6-P]			μM	50	-7×10^{-6}

[a] Equation number where parameter is related to rate constants.
[b] Flux response coefficients of the parameters (R_p^J) were calculated as described under "Appendix."

tion is uncomplexed. This is in agreement with the control theory (12), which relates R^J_{PTS} values approaching 2 to the absence of protein-protein complexes and R^J_{PTS} values near 1 to the prevalence of these complexes in significant proportions. In fact, complexes between HPr and IIA$^{\mathrm{Glc}}$ (40), as well as IIA$^{\mathrm{Glc}}$ and IICB$^{\mathrm{Glc}}$ (53) have been demonstrated biochemically, although both proteins were unphosphorylated. It is likely that their interaction will be much stronger if one of the two proteins is phosphorylated, since this situation obtains during the normal sequence of phosphotransfer along the PTS. Therefore, complexes between the PTS proteins may well exist for significant lifetimes in the cell.

Table III shows that only 1.6% of the total IIA$^{\mathrm{Glc}}$ exists in the free unphosphorylated state when simulating MeGlc uptake *in vivo*. The question arises how the PTS can still regulate other systems by inducer exclusion under these conditions, because unphosphorylated IIA$^{\mathrm{Glc}}$ binds stoichiometrically to its target proteins. Additional simulations (54) have shown that introduction of a step for binding of free unphosphorylated IIA$^{\mathrm{Glc}}$ to a target protein leads to a redistribution of the IIA$^{\mathrm{Glc}}$ forms and that a significant fraction of the total IIA$^{\mathrm{Glc}}$ can bind to the target protein if the dissociation equilibrium constant is in the range of 0.2–1 μM, as reported for glycerol kinase and IIA$^{\mathrm{Glc}}$ in the presence of Zn(II) (55). However, the addition of glucose by itself to a suspension of *E. coli* cells (*i.e.* under non-inducer exclusion conditions) has been shown to lead to >95% dephosphorylation of IIA$^{\mathrm{Glc}}$ after 15 s (33). How does this relate to the 39% IIA$^{\mathrm{Glc}}$·P (*i.e.* $\gg$5%) calculated by the model when simulating glucose (or MeGlc) uptake *in vivo* (Table III)? One explanation can certainly be based on the intracellular concentrations of PEP and pyruvate, and specifically their ratio, which drops from 3.0 to less than 0.1 after the cells have been challenged with glucose for 15 s and recovers to 0.2 after 30 s (33). Using these PEP and pyruvate concentrations, the model predicts IIA$^{\mathrm{Glc}}$ · P to be 7% of the total IIA$^{\mathrm{Glc}}$ 15 s after glucose addition (14% after 30 s), which agrees much better with the experimental results. Why did we not use the lower PEP/pyruvate ratios in our simulations? It is a well known fact that the PTS-mediated MeGlc uptake rate decreases with time (the slope of the curve decreases), and to ensure that we simulate *initial* uptake rates, we entered the concentrations of PEP and pyruvate in the model as they were determined just prior to glucose addition.

The second-order rate constant for phosphotransfer between HPr and IIA$^{\mathrm{Glc}}$ reported by Meadow and Roseman (6) (6.1×10^7 M^{-1} s^{-1}) is much larger than the value of 6×10^6 M^{-1} min^{-1} (10^5 M^{-1} s^{-1}) reported by Misset *et al.* (56). The larger value is essential for obtaining the results presented here. Using the lower value of Misset *et al.*, the simulated flux was significantly lower, and the flux response coefficients of EI and HPr were significantly higher, which did not match the experimental results (data not shown). We conclude, therefore, that the use of the second order rate constant of IIA$^{\mathrm{Glc}}$ phosphorylation reported in Ref. 56 in our kinetic model yielded results that did not correspond with the strain and conditions used in the experiments determining the flux response coefficients *in vivo* and that the experimental improvement of measuring the phosphotransfer directly between the two proteins (6) resulted in values that improved the fit of the model to MeGlc uptake data *in vivo*. In contrast, the second order rate constant of EI phosphorylation by PEP (2×10^8 to 10^9 M^{-1} min^{-1} = 200–1000 $\mu\mathrm{M}^{-1}$ min^{-1}) reported in Ref. 47 agrees very well with the 360 $\mu\mathrm{M}^{-1}$ min^{-1} found by Meadow and Roseman.[2]

Remarkably, the effects of the macromolecular crowding agent PEG 6000 on PTS activity *in vitro* could be simulated with the kinetic model by assuming increased on-rates for protein-protein complex formation and decreased off-rates for its dissociation. An increased relative fraction of complexes between the proteins could in principle be achieved by increasing the on-rates for complex formation or by decreasing the off-rates for complex

[2] N. D. Meadow and S. Roseman, unpublished results.

dissociation or both. Minton (57) has argued on thermodynamic grounds that the association of monomers to homopolymers should be stimulated by the addition of crowding agents mainly via an enhancement of the on-rate. As reasoned in Ref. 11, however, PEG 6000 resulted in both a stimulation and an inhibition of the flux, depending on the protein concentration, and this can only be achieved by a simultaneous effect on *both* the on-rate and the off-rate. Indeed, even for the simplistic assumption that the on-rate and off-rate constants are affected to the same extent (but in opposite directions) by PEG 6000 addition and furthermore that complex formation between the different PTS proteins is enhanced to the *same* extent, the agreement between model and experiment was remarkable when comparing the effect of two PEG 6000 concentrations with two values for the parameter α, *i.e.* the factor by which the rate constants are affected (*cf.* Fig. 1 in Ref. 11 and Fig. 2*a* in this paper). It may be noted that when calculating the PTS transport rate *in vivo*, we set the crowding parameter α to 1, *i.e.* implying that we used the concentrations of PTS proteins on the basis of number of molecules per intracellular cytoplasmic volume without taking into account the volume exclusion effects accompanying macromolecular crowding. In parallel calculations (not shown here), we set α to values different from 1. The results were closer to experimental observations on some counts but farther off on others. More *in vivo* experimental work is needed; our model may be helpful here.

The comprehensive kinetic model of the PTS presented in this paper may be used to predict the flux through the PTS for different induction levels of the glucose PTS proteins. Furthermore, the phosphorylation states of all the proteins (*i.e.* the ratio between the phosphorylated and unphosphorylated forms) can be computed, which has important implications for signaling (*e.g.* by IIA^{Glc} in inducer exclusion and the activation of adenylate cyclase). There is a distinct possibility for improvement and further validation of the model by measuring the phosphorylation state of IIA^{Glc} under different conditions, as described in Ref. 33, and comparing the results with the model predictions. We have used only flux data to assess the performance of the model in describing experimental results; inclusion of the concentrations of the phosphorylated and unphosphorylated protein forms should be an interesting and valuable addition. We have presented preliminary reports (54) on the use of the kinetic model to simulate the interaction of the signal transducer IIA^{Glc} with its target proteins under conditions that lead to the phenomena of inducer exclusion (2) and reverse inducer exclusion (58). An ambitious goal is the incorporation of the present model in a much larger model describing the glycolysis of enteric bacteria. Realization of such a project should provide interesting new insights into metabolic regulation, especially since glycolysis following PTS-mediated uptake differs from that in other organisms in that the phosphoryl donor for the initial carbohydrate phosphorylation during PTS-mediated uptake is PEP and not ATP.

The kinetic equations presented here are a first step in devising a testable model for quantifying sugar uptake by the PTS, and we have used a particular set of conditions (*i.e.* glucose-grown cells) to test the model. However, the model is adaptable to other experimental conditions, for instance with cells grown on other carbon sources or with leaky mutant PTS proteins, provided that the necessary parameters are defined. Under such conditions, it may well be that PTS proteins other than $IICB^{Glc}$ become the major rate determinants for sugar uptake. For instance, in the extreme case, if EI were all monomer or was somehow converted to all monomer, sugar uptake would halt. The importance of the present model is that it can readily be adjusted to account for unknown factors that affect functioning of the PTS as they are characterized and their kinetic effects are determined *in vitro*. These factors can include regulators on the genetic level; *e.g.* Mlc, a negative regulator of the *ptsHI* operon and *ptsG*, has recently been proposed to bind to unphosphorylated $IICB^{Glc}$, so that conditions leading to $IICB^{Glc}$ dephosphorylation (glucose transport, *ptsHIcrr* deletion) may result in $IICB^{Glc}$ sequestering Mlc, leading to *ptsHI* and *ptsG* activation (59).

Since signal transduction along two-component regulatory systems (14, 15) involves phosphoryl transfer similar to the PTS, our modeling results suggest that complex formation between the different signaling proteins may well be expected to occur as well. This could strongly influence their control properties in that the combined flux response, and thus the speed of signal transmission, depends on macromolecular crowding and differs between intracellular conditions and dilute solutions *in vitro*. Furthermore, this pattern of signal transfer is not limited to prokaryotes. For example, phosphoryl transfer through the components of a two-component system was demonstrated to be part of the osmosensing response in yeast (60). In addition, a chimeric protein consisting of the sensing domain of the *E. coli* aspartate receptor and the cytosolic portion of the human insulin receptor was able to activate the insulin pathway in response to aspartate (61), demonstrating the generality of the signal transfer mechanism. Therefore, the novel aspects of metabolic behavior described in this paper may also apply to eukaryotic signal transduction. Most importantly, we show here how it is possible to analyze these systems quantitatively, in order to assess their properties and predict their dynamic behavior in the living cell.

Acknowledgments—We thank Rechien Bader-van't Hof for performing PTS phosphorylation assays and Jannie Hofmeyr and Boris Kholodenko for helpful discussions.

APPENDIX

Metabolic Control Analysis

Metabolic control analysis is a quantitative framework originally developed by Kacser and Burns (7) and Heinrich and Rapoport (8) to quantify the control of the steady-state behavior of metabolic systems. An important entity in this analysis is the so-called flux response coefficient, which quantifies the extent to which a change in a parameter of a metabolic pathway affects the flux through that pathway and is defined mathematically as follows,

$$R^J_{p_j} = \left(\frac{\partial J}{\partial p_j}\right)_{p_k} \cdot \frac{p_j}{J} = \left(\frac{\partial \ln|J|}{\partial \ln p_j}\right)_{p_k} \quad \text{(Eq. 8)}$$

where J is the steady-state flux through the pathway and p_j is the modulated parameter. Operationally, $R^J_{p_j}$ can be envisaged as the percentage change in J upon a 1% increase in p_j. The parameter p_j can, for example, be the concentration of an external metabolite that affects the pathway flux or the concentration of an enzyme in the pathway. When measuring a flux response coefficient, the system is allowed to relax to a new steady state after perturbation in the parameter p_j while keeping all of the other parameters p_k constant, as indicated by subscript p_k.

The extent to which any catalytic component (*e.g.* an elementary step of a reaction mechanism) controls the flux is quantified by a control coefficient, which, for a step i of the system, is defined (62) as follows,

$$C^J_i = \frac{(\partial \ln|J|/\partial p_i)_{p_k}}{(\partial \ln|v_i|/\partial p_i)_{s_j,\, p_k}} \quad \text{(Eq. 9)}$$

where p_i is any parameter that affects step i specifically. Subscript p_k indicates, as above, that the other parameters p_k remain constant and that the entire system relaxes to a new

steady state after a change in p_i; subscript s_j, p_k indicates that the change in the rate v_i of the independent step i is considered locally at constant reactant and product concentrations (63). For step i, referring to an elementary reaction in an enzyme mechanism (as the individual phosphotransfer reactions of the PTS), the control coefficient has also been termed the friction coefficient (64).

Derivation of Rate Constants for PTS Reactions

Here we derive elementary rate constants, as shown in Scheme 2 under "Materials and Methods," for the five phosphotransfer reactions of the glucose PTS from available kinetic data for the PTS components, using the relationships in Equations 1–7. In some cases, insufficient data were available, and additional assumptions had to be made, as indicated clearly. To ensure that all quantities were expressed in the same units, we consistently converted all concentrations to micromolar and all time units to minutes.

Phosphotransfer from Phosphoenolpyruvate to EI—The first phosphotransfer reaction from PEP to EI can be written schematically as follows,

$$\mathrm{EI} + \mathrm{PEP} \underset{k_{-\mathrm{I}}}{\overset{k_{\mathrm{I}}}{\rightleftharpoons}} \mathrm{EI \cdot P} + \mathrm{Pyr}$$

SCHEME 3

$$\mathrm{EI} + \mathrm{PEP} \underset{k_{-1}}{\overset{k_1}{\rightleftharpoons}} \mathrm{EI \cdot P \cdot Pyr} \underset{k_{-2}}{\overset{k_2}{\rightleftharpoons}} \mathrm{EI \cdot P} + \mathrm{Pyr}$$

SCHEME 4

where Scheme 3 shows the direct phosphotransfer and Scheme 4 includes the complex EI·P·Pyr explicitly.

Reported K_m values of Scheme 4 (*i.e.* of EI for PEP) range from 0.2 to 0.4 mM (43, 65), and values of EI · P for Pyr range from 1.5 to 3 mM (66). Furthermore, the equilibrium constant for the above reaction is 1.5 (44). Using a rapid quench method as described in Ref. 6, the forward rate constant of the overall phosphorylation reaction (*i.e.* k_{I} in Scheme 3) has been determined as $6 \times 10^6\ \mathrm{M^{-1}\,s^{-1}}$.[3] Selecting values of 0.3 and 2 mM for $K_{m\mathrm{PEP}}$ and $K_{m\mathrm{Pyr}}$, respectively, the following set of equations can be derived using the approaches outlined under "Materials and Methods."

$$K_{m\mathrm{PEP}} = \frac{k_{-1} + k_2}{k_1} = 300\ \mu\mathrm{M} \qquad \text{(Eq. 10)}$$

$$K_{m\mathrm{Pyr}} = \frac{k_{-1} + k_2}{k_{-2}} = 2000\ \mu\mathrm{M} \qquad \text{(Eq. 11)}$$

$$K_{\mathrm{eqI}} = \frac{k_{\mathrm{I}}}{k_{-1}} = \frac{k_1 k_2}{k_{-1} k_{-2}} = 1.5 \qquad \text{(Eq. 12)}$$

$$k_I = \frac{k_1 k_2}{k_{-1} + k_2} = 6 \times 10^6\ \mathrm{M^{-1}s^{-1}} = 360\ \mu\mathrm{M^{-1}min^{-1}} \qquad \text{(Eq. 13)}$$

Equations 10–13 can be solved simultaneously for the elementary rate constants k_1, k_{-1}, k_2, and k_{-2} of Scheme 4 as follows.

$$k_1 = \frac{k_{\mathrm{I}}[K_{\mathrm{eqI}} K_{m\mathrm{PEP}} + K_{m\mathrm{Pyr}}]}{K_{\mathrm{eqI}} K_{m\mathrm{PEP}}} = 1960\ \mu\mathrm{M^{-1}min^{-1}} \qquad \text{(Eq. 14)}$$

$$k_{-1} = \frac{k_{\mathrm{I}} K_{m\mathrm{Pyr}}}{K_{\mathrm{eqI}}} = 480{,}000\ \mathrm{min^{-1}} \qquad \text{(Eq. 15)}$$

$$k_2 = k_{\mathrm{I}} K_{m\mathrm{PEP}} = 108{,}000\ \mathrm{min^{-1}} \qquad \text{(Eq. 16)}$$

[3] N. D. Meadow and S. Roseman, unpublished results.

$$k_{-2} = \frac{k_{\mathrm{I}}[K_{\mathrm{eqI}} K_{m\mathrm{PEP}} + K_{m\mathrm{Pyr}}]}{K_{\mathrm{eqI}} K_{m\mathrm{Pyr}}} = 294\ \mu\mathrm{M^{-1}min^{-1}} \qquad \text{(Eq. 17)}$$

Phosphotransfer from EI to HPr—The second phosphotransfer reaction from phosphorylated EI to HPr can be written schematically as follows.

$$\mathrm{EI \cdot P} + \mathrm{HPr} \underset{k_{-\mathrm{II}}}{\overset{k_{\mathrm{II}}}{\rightleftharpoons}} \mathrm{EI} + \mathrm{HPr \cdot P}$$

SCHEME 5

$$\mathrm{EI \cdot P} + \mathrm{HPr} \underset{k_{-3}}{\overset{k_3}{\rightleftharpoons}} \mathrm{EI \cdot P \cdot HPr} \underset{k_{-4}}{\overset{k_4}{\rightleftharpoons}} \mathrm{EI} + \mathrm{HPr \cdot P}$$

SCHEME 6

Again, the former reaction, Scheme 5, describes direct phosphotransfer, whereas the latter (Scheme 6) includes the complex EI · P · HPr explicitly.

Reported K_m^* values of EI for HPr range from 2.7 to 9 μM (43, 65, 67–69); we shall assume a value of 7 μM here. The association constant K_a for EI and HPr is $10^5\ \mathrm{M^{-1}}$ (abstract cited in Ref. 1), although this most probably refers to the interaction between unphosphorylated EI and HPr. The interaction between a phosphorylated and an unphosphorylated protein is likely to be stronger than that between two unphosphorylated proteins, since the former situation obtains during the normal phosphotransfer reaction sequence. Recently, the rate constants of the overall phosphorylation reaction (Scheme 5) were determined directly using the rapid quench method (see above): $k_{\mathrm{II}} = 2 \times 10^8\ \mathrm{M^{-1}\,s^{-1}}$ and $k_{-\mathrm{II}} = 8 \times 10^6\ \mathrm{M^{-1}\,s^{-1}}$.[2] The equilibrium constant for phosphotransfer from EI to HPr, as calculated from k_{II} and $k_{-\mathrm{II}}$, is 25; this value is higher than the 2.3–8.9 reported previously (44). Because of their direct determination, we shall use the above values for k_{II} and $k_{-\mathrm{II}}$ and 25 for $K_{\mathrm{eq\ II}}$. The combined equilibrium constant for the first two PTS reactions (*i.e.* phosphotransfer from PEP to HPr) is $1.5 \times 25 = 37.5$ when proceeding from the measured rate constants, which likewise exceeds the experimental value of 10.8 ± 7.7 reported previously (44).

We can derive the following set of equations.

$$K_{m\mathrm{HPr}}^* = \frac{k_{-3} + k_4}{k_3} = 7\ \mu\mathrm{M} \qquad \text{(Eq. 18)}$$

$$k_{\mathrm{II}} = \frac{k_3 k_4}{k_{-3} + k_4} = 2 \times 10^8\ \mathrm{M^{-1}s^{-1}} = 12{,}000\ \mu\mathrm{M^{-1}min^{-1}} \qquad \text{(Eq. 19)}$$

$$k_{-\mathrm{II}} = \frac{k_{-3} k_{-4}}{k_{-3} + k_4} = 8 \times 10^6\ \mathrm{M^{-1}s^{-1}} = 480\ \mu\mathrm{M^{-1}min^{-1}} \qquad \text{(Eq. 20)}$$

Equations 18–20 contain insufficient information to solve for the rate constants k_3, k_{-3}, k_4, and k_{-4} unambiguously. Some additional choice has to be made for k_3, k_{-3}, or k_{-4}. For example, fixing the association equilibrium constant K_a of EI·P and HPr allows calculation of all of the rate constants. We assumed the association of EI·P and HPr to be 10-fold stronger that that of unphosphorylated EI and HPr,

$$K_{a\mathrm{II}} = k_3/k_{-3} = 10^6\ \mathrm{M^{-1}} = 1\ \mu\mathrm{M^{-1}} \qquad \text{(Eq. 21)}$$

This yields the following rate constants for the elementary steps in Scheme 6.

$$k_3 = \frac{K_{m\mathrm{HPr}}^* K_{a\mathrm{III}} k_{\mathrm{II}}}{K_{m\mathrm{HPr}}^* K_{a\mathrm{III}} - 1} = 14{,}000\ \mu\mathrm{M^{-1}min^{-1}} \qquad \text{(Eq. 22)}$$

$$k_{-3} = \frac{K_{m\mathrm{HPr}}^* k_{\mathrm{II}}}{K_{m\mathrm{HPr}}^* K_{a\mathrm{III}} - 1} = 14{,}000\ \mathrm{min^{-1}} \qquad \text{(Eq. 23)}$$

$$k_4 = K^*_{m\mathrm{HPr}} k_{\mathrm{II}} = 84{,}000\ \mathrm{min}^{-1} \quad \text{(Eq. 24)}$$

$$k_{-4} = K^*_{m\mathrm{HPr}} K_{a\mathrm{III}} k_{-\mathrm{II}} = 3360\ \mu\mathrm{M}^{-1}\mathrm{min}^{-1} \quad \text{(Eq. 25)}$$

Phosphotransfer from HPr to IIA^{Glc}—The third phosphotransfer reaction from phosphorylated HPr to IIA^{Glc} can be written schematically as follows.

$$\mathrm{HPr}\cdot\mathrm{P} + \mathrm{IIA}^{\mathrm{Glc}} \underset{k_{-\mathrm{III}}}{\overset{k_{\mathrm{III}}}{\rightleftharpoons}} \mathrm{HPr} + \mathrm{IIA}^{\mathrm{Glc}}\cdot\mathrm{P}$$

SCHEME 7

$$\mathrm{HPr}\cdot\mathrm{P} + \mathrm{IIA}^{\mathrm{Glc}} \underset{k_{-5}}{\overset{k_5}{\rightleftharpoons}} \mathrm{HPr}\cdot\mathrm{P}\cdot\mathrm{IIA}^{\mathrm{Glc}} \underset{k_{-6}}{\overset{k_6}{\rightleftharpoons}} \mathrm{HPr} + \mathrm{IIA}^{\mathrm{Glc}}\cdot\mathrm{P}$$

SCHEME 8

As above, Scheme 7 shows the direct phosphotransfer, and Scheme 8 includes the complex HPr · P · IIA^{Glc} explicitly.

Values of 0.3 μM (69) and 2.7 μM (56) have been reported for the K^*_m of IIA^{Glc} for HPr·P. The association constant K_a for HPr and IIA^{Glc} was measured as 10^4 to 10^5 M^{-1} (40); however, this was measured for unphosphorylated HPr, not HPr·P. As for the interaction between EI and HPr, the K_a of HPr·P and IIA^{Glc} will most probably be larger than that for unphosphorylated HPr and IIA^{Glc} because HPr·P donates a phosphoryl group to IIA^{Glc} during the normal phosphotransfer reaction sequence. The rate constants for the overall phosphorylation reaction (Scheme 7) have been published: $k_{\mathrm{III}} = 6.1 \times 10^7$ M^{-1} s^{-1} and $k_{-\mathrm{III}} = 4.7 \times 10^7$ M^{-1} s^{-1} (6). The equilibrium constant for phosphotransfer from HPr to IIA^{Glc}, as calculated from k_{III} and $k_{-\mathrm{III}}$, is 1.3; this value is 10-fold higher than the 0.13 reported previously (70).

Assuming a value of 1.2 μM for the K^*_m of IIA^{Glc} for HPr · P and using the directly determined rate constants, we can derive the following set of equations.

$$K^*_{m\mathrm{HPr}\cdot\mathrm{P}} = \frac{k_{-5} + k_6}{k_5} = 1.2\ \mu\mathrm{M} \quad \text{(Eq. 26)}$$

$$k_{\mathrm{III}} = \frac{k_5 k_6}{k_{-5} + k_6} = 6.1 \times 10^7\ \mathrm{M}^{-1}\mathrm{s}^{-1} = 3660\ \mu\mathrm{M}^{-1}\mathrm{min}^{-1} \quad \text{(Eq. 27)}$$

$$k_{-\mathrm{III}} = \frac{k_{-5} k_{-6}}{k_{-5} + k_6} = 4.7 \times 10^7\ \mathrm{M}^{-1}\mathrm{s}^{-1} = 2820\ \mu\mathrm{M}^{-1}\mathrm{min}^{-1} \quad \text{(Eq. 28)}$$

As was the case for phosphotransfer between EI and HPr, Equations 26–28 contain insufficient information to solve for the rate constants k_5, k_{-5}, k_6, and k_{-6} unambiguously. We here assumed additionally a value of 1 μM^{-1} for the association constant of HPr · P and IIA^{Glc}. This is identical to the association constant of EI · P and HPr, and 10–100-fold larger than the association constant of unphosphorylated HPr and IIA^{Glc} (see above). With the additional assumption,

$$K_{a\mathrm{III}} = k_5/k_{-5} = 1\ \mu\mathrm{M}^{-1} \quad \text{(Eq. 29)}$$

and using Equations 26–28, the following rate constants for the elementary steps in Scheme 8 were calculated.

$$k_5 = \frac{K_{a\mathrm{III}} k_{\mathrm{III}} K^*_{m\mathrm{HPr}\cdot\mathrm{P}}}{K_{a\mathrm{III}} K^*_{m\mathrm{HPr}\cdot\mathrm{P}} - 1} = 21{,}960\ \mu\mathrm{M}^{-1}\mathrm{min}^{-1} \quad \text{(Eq. 30)}$$

$$k_{-5} = \frac{k_{\mathrm{III}} K^*_{m\mathrm{HPr}\cdot\mathrm{P}}}{K_{a\mathrm{III}} K^*_{m\mathrm{HPr}\cdot\mathrm{P}} - 1} = 21{,}960\ \mathrm{min}^{-1} \quad \text{(Eq. 31)}$$

$$k_6 = k_{\mathrm{III}} K^*_{m\mathrm{HPr}\cdot\mathrm{P}} = 4392\ \mathrm{min}^{-1} \quad \text{(Eq. 32)}$$

$$k_{-6} = K_{a\mathrm{III}} k_{-\mathrm{III}} K^*_{m\mathrm{HPr}\cdot\mathrm{P}} = 3384\ \mu\mathrm{M}^{-1}\mathrm{min}^{-1} \quad \text{(Eq. 33)}$$

However, we have reservations about both published values for $K^*_{m\ \mathrm{HPr}\cdot\mathrm{P}}$. In order for the assay conditions in the paper by Reizer *et al.* (69) to measure the K_m of the reaction that the authors claim, all of the HPr must have been phosphorylated, whereas all of the IIA^{Glc} must have been dephosphorylated. Whereas the former condition may well have been true, one cannot assume that the latter condition always held, because of (*a*) the speed of the HPr·P-IIA^{Glc} phosphotransfer reaction and (*b*) the low concentrations of IICB^{Glc} used in comparison with the higher HPr concentrations. In the paper by Misset *et al.* (56), the fact that no IIA^{Glc} was added to the assays calls into question just which PTS was being measured, especially in the light of the structural similarity and functional exchangeability of the IIA domains of various sugar-specific systems (see *e.g.* Refs. 71 and 72). For these reasons, we also modeled phosphoryl transfer between HPr·P and IIA^{Glc} as a direct reaction (Scheme 7), using the published values of k_{III} and $k_{-\mathrm{III}}$, and omitting $K^*_{m\ \mathrm{HPr}\cdot\mathrm{P}}$ (Equation 26) as well as the assumption of K_a (Equation 29). The modeling results did not differ significantly from the ones presented in Figs. 1 and 2 (data not shown). For reasons of consistency, we therefore modeled all five phosphotransfer reactions as proceeding via an explicit transition state complex.

Phosphotransfer from IIA^{Glc} to IICB^{Glc}—The fourth phosphotransfer reaction from phosphorylated IIA^{Glc} to IICB^{Glc} can be written schematically as follows.

$$\mathrm{IIA}^{\mathrm{Glc}}\cdot\mathrm{P} + \mathrm{IICB}^{\mathrm{Glc}} \underset{k_{-\mathrm{IV}}}{\overset{k_{\mathrm{IV}}}{\rightleftharpoons}} \mathrm{IIA}^{\mathrm{Glc}} + \mathrm{IICB}^{\mathrm{Glc}}\cdot\mathrm{P}$$

SCHEME 9

$$\mathrm{IIA}^{\mathrm{Glc}}\cdot\mathrm{P} + \mathrm{IICB}^{\mathrm{Glc}} \underset{k_{-7}}{\overset{k_7}{\rightleftharpoons}} \mathrm{IIA}^{\mathrm{Glc}}\cdot\mathrm{P}\cdot\mathrm{IICB}^{\mathrm{Glc}} \underset{k_{-8}}{\overset{k_8}{\rightleftharpoons}} \mathrm{IIA}^{\mathrm{Glc}} + \mathrm{IICB}^{\mathrm{Glc}}\cdot\mathrm{P}$$

SCHEME 10

Scheme 9 shows the direct phosphotransfer, and Scheme 10 includes the transition state complex IIA^{Glc}·P·IICB^{Glc} explicitly.

The K^*_m of IICB^{Glc} for IIA^{Glc}·P ranges from 1.7 to 5 μM (22, 69, 70, 73). Recently, the rate constants of the overall phosphorylation reaction (Scheme 9) were determined directly using the rapid quench method (see above): $k_{\mathrm{IV}} = 1.1 \times 10^7$ M^{-1} s^{-1} and $k_{-\mathrm{IV}} = 4 \times 10^6$ M^{-1} s^{-1}.[3] Using these rate constants and a value of 4 μM for $K^*_{m\ \mathrm{IIAGlc}\cdot\mathrm{P}}$ yields three equations.

$$K^*_{m\mathrm{IIAGlc}\cdot\mathrm{P}} = \frac{k_{-7} + k_8}{k_7} = 4\ \mu\mathrm{M} \quad \text{(Eq. 34)}$$

$$k_{\mathrm{IV}} = \frac{k_7 k_8}{k_{-7} + k_8} = 1.1 \times 10^7\ \mathrm{M}^{-1}\mathrm{s}^{-1} = 660\ \mu\mathrm{M}^{-1}\mathrm{min}^{-1} \quad \text{(Eq. 35)}$$

$$k_{-\mathrm{IV}} = \frac{k_{-7} k_{-8}}{k_{-7} + k_8} = 4 \times 10^6\ \mathrm{M}^{-1}\mathrm{s}^{-1} = 240\ \mu\mathrm{M}^{-1}\mathrm{min}^{-1} \quad \text{(Eq. 36)}$$

No additional literature data were found. In order to solve for the rate constants k_7, k_{-7}, k_8, and k_{-8}, one further independent equation (*i.e.* one assumption) is needed as above. We assumed an association constant of 1 μM^{-1} for IIA^{Glc} · P and IICB^{Glc} (identical to the association constants of EI · P and HPr and of HPr · P and IIA^{Glc}). This yielded the following additional equation,

$$K_{a\mathrm{IV}} = k_7/k_{-7} = 1\ \mu\mathrm{M}^{-1} \quad \text{(Eq. 37)}$$

which, together with Equations 34–36, was solved simultaneously for the rate constants of the elementary steps in scheme 10 as follows.

$$k_7 = \frac{K_{a\mathrm{IV}} k_{\mathrm{IV}} K^*_{m\mathrm{IIAGlc}\cdot\mathrm{P}}}{K_{a\mathrm{IV}} K^*_{m\mathrm{IIAGlc}\cdot\mathrm{P}} - 1} = 880\ \mu\mathrm{M}^{-1}\mathrm{min}^{-1} \quad \text{(Eq. 38)}$$

[3] N. D. Meadow, R. Savtchenko, and S. Roseman, unpublished results.

$$k_{-7} = \frac{k_{IV}K^*_{mIIAGlc\cdot P}}{K_{aIV}K^*_{mIIAGlc\cdot P} - 1} = 880\ \text{min}^{-1} \quad \text{(Eq. 39)}$$

$$k_8 = k_{IV}K^*_{mIIAGlc\cdot P} = 2640\ \text{min}^{-1} \quad \text{(Eq. 40)}$$

$$k_{-8} = K_{aIV}k_{-IV}K^*_{mIIAGlc\cdot P} = 960\ \mu\text{M}^{-1}\text{min}^{-1} \quad \text{(Eq. 41)}$$

Phosphotransfer from IICB^{Glc} to Glucose—The fifth and final phosphotransfer reaction from phosphorylated IICB^{Glc} to glucose (Glc) can be written schematically as follows.

$$IICB^{Glc}\cdot P + Glc \underset{k_{-V}}{\overset{k_V}{\rightleftharpoons}} IICB^{Glc} + Glc\cdot P$$

SCHEME 11

$$IICB^{Glc}\cdot P + Glc \underset{k_{-9}}{\overset{k_9}{\rightleftharpoons}} IICB^{Glc}\cdot P\cdot Glc \underset{k_{-10}}{\overset{k_{10}}{\rightleftharpoons}} IICB^{Glc} + Glc\cdot P$$

SCHEME 12

As previously, Scheme 11 shows the direct phosphotransfer, and Scheme 12 includes the complex IICB^{Glc}·P · Glc explicitly. Note that during PTS-mediated uptake, the substrate is phosphorylated concomitantly with the uptake process, so that Glc above refers to extracellular glucose, whereas Glc · P refers to intracellular glucose 6-phosphate.

The K_m of IICB^{Glc} for glucose is 10 μM *in vitro* and 20 μM in an uptake assay *in vivo* (41). The dissociation constant K_d of glucose from IICB^{Glc} is 1.5 μM (42). The equilibrium constant K_{eqV} for Scheme 11 was taken as 5.9×10^5. This was calculated from the equilibrium constant of $10^{7.9}$ for phosphoryl transfer along the complete PTS from PEP to glucose (44) and from the equilibrium constants for each of the other phosphoryl transfer reactions. The forward overall rate constant of Scheme 11 was determined recently using the rapid quench method (see above): $k_V = 4 \times 10^6\ \text{M}^{-1}\ \text{s}^{-1}$.[3]

It should be noted that the kinetic parameters for glucose and not for MeGlc (its nonmetabolizable analogue) were used in this derivation, although MeGlc was used for both the uptake experiments *in vivo* (9) and the flux analyses *in vitro* (11). The reasons for this were 2-fold. First, there was a large discrepancy between reported K_m values for MeGlc (170 μM *in vivo* and 6 μM *in vitro*) (41), whereas the K_m values for glucose agreed much better (see above). Second, the K_d value (Equation 43) has only been determined for glucose (42) (also see "Discussion").

Using 20 μM for the K_m of IICB^{Glc} for glucose and the K_{dGlc}, K_{eqV}, and k_V values above, the following set of equations,

$$K_{mGlc} = \frac{k_{-9} + k_{10}}{k_9} = 20\ \mu\text{M} \quad \text{(Eq. 42)}$$

$$K_{dGlc} = k_{-9}/k_9 = 1.5\ \mu\text{M} \quad \text{(Eq. 43)}$$

$$K_{eqV} = \frac{k_V}{k_{-V}} = \frac{k_9k_{10}}{k_{-9}k_{-10}} = 5.9 \times 10^5 \quad \text{(Eq. 44)}$$

$$k_V = \frac{k_9k_{10}}{k_{-9} + k_{10}} = 4 \times 10^6\ \text{M}^{-1}\text{s}^{-1} = 240\ \mu\text{M}^{-1}\text{min}^{-1} \quad \text{(Eq. 45)}$$

was solved simultaneously to calculate the rate constants of the elementary steps in Scheme 12,

$$k_9 = \frac{k_VK_{mGlc}}{K_{mGlc} - K_{dGlc}} = 260\ \mu\text{M}^{-1}\text{min}^{-1} \quad \text{(Eq. 46)}$$

$$k_{-9} = \frac{k_VK_{mGlc}K_{dGlc}}{K_{mGlc} - K_{dGlc}} = 389\ \text{min}^{-1} \quad \text{(Eq. 47)}$$

$$k_{10} = k_VK_{mGlc} = 4800\ \text{min}^{-1} \quad \text{(Eq. 48)}$$

$$k_{-10} = \frac{k_VK_{mGlc}}{K_{eqV}K_{dGlc}} = 5.4 \times 10^{-3}\ \mu\text{M}^{-1}\text{min}^{-1} \quad \text{(Eq. 49)}$$

Parameter Sensitivity Analysis

The flux response coefficients toward the model parameters in Table IV were calculated as follows. Consider, as an example, $R^J_{K_{mPEP}}$ (*i.e.* the parameter sensitivity toward K_{mPEP}). From Equation 8 we have the following,

$$\begin{aligned} R^J_{K_{mPEP}} &= \left(\frac{\partial \ln|J|}{\partial \ln K_{mPEP}}\right)_{pk} \\ &= R^J_{k_1}\left(\frac{\partial \ln k_1}{\partial \ln K_{mPEP}}\right)_{pk} + R^J_{k_{-1}}\left(\frac{\partial \ln k_{-1}}{\partial \ln K_{mPEP}}\right)_{pk} \\ &\quad + R^J_{k_2}\left(\frac{\partial \ln k_2}{\partial \ln K_{mPEP}}\right)_{pk} + R^J_{k_{-2}}\left(\frac{\partial \ln k_{-2}}{\partial \ln K_{mPEP}}\right)_{pk} \end{aligned} \quad \text{(Eq. 50)}$$

The flux response coefficients $R^J_{k_1}$, $R^J_{k_{-1}}$, $R^J_{k_2}$, and $R^J_{k_{-2}}$ in Equation 50 were calculated directly by the program SCAMP using the *Fluxsensitivity* feature. The other derivatives were calculated from the expressions for the rate constants derived above. Consider the first term as an example. From Equation 14 we have the following.

$$\ln k_1 = \ln k_I + \ln[K_{eqI}K_{mPEP} + K_{mPyr}] - \ln K_{eqI} - \ln K_{mPEP} \quad \text{(Eq. 51)}$$

Differentiating partially,

$$\begin{aligned} \frac{\partial \ln k_1}{\partial \ln K_{mPEP}} &= -1 + \frac{K_{eqI}K_{mPEP}}{K_{eqI}K_{mPEP} + K_{mPyr}} = \frac{-K_{mPyr}}{K_{eqI}K_{mPEP} + K_{mPyr}} \\ &= \frac{-2000}{1.5 \times 300 + 2000} = -0.82 \end{aligned} \quad (52)$$

The other derivatives were calculated similarly, enabling determination of the flux response coefficient $R^J_{K_{mPEP}}$ using Equation 50. The other parameter sensitivities in Table IV were obtained by following a similar approach.

REFERENCES

1. Meadow, N. D., Fox, D. K., and Roseman, S. (1990) *Annu. Rev. Biochem.* **59,** 497–542
2. Postma, P. W., Lengeler, J. W., and Jacobson, G. R. (1996) in *Cellular and Molecular Biology* (Neidhardt, F. C., Curtiss, R., III, Ingraham, J. L., Lin, E. C. C., Low, K. B., Magasanik, B., Reznikoff, W. S., Riley, M., Schaechter, M., and Umbarger, H. E., eds) 2nd Ed., Vol. 1, pp. 1149–1174, American Society for Microbiology, Washington, D. C.
3. Robillard, G. T., and Lolkema, J. S. (1988) *Biochim. Biophys. Acta* **947,** 493–519
4. Lengeler, J. W., Jahreis, K., and Wehmeier, U. F. (1994) *Biochim. Biophys. Acta* **1188,** 1–28
5. Saier, Jr., M. H. (1989) *Microbiol. Rev.* **53,** 109–120
6. Meadow, N. D., and Roseman, S. (1996) *J. Biol. Chem.* **271,** 33440–33445
7. Kacser, H., and Burns, J. A. (1973) *Symp. Soc. Exp. Biol.* **27,** 65–104
8. Heinrich, R., and Rapoport, T. A. (1974) *Eur. J. Biochem.* **42,** 89–95
9. van der Vlag, J., van't Hof, R., van Dam, K., and Postma, P. W. (1995) *Eur. J. Biochem.* **230,** 170–182
10. Ruijter, G. J. G., Postma, P. W., and van Dam, K. (1991) *J. Bacteriol.* **173,** 6184–6191
11. Rohwer, J. M., Postma, P. W., Kholodenko, B. N., and Westerhoff, H. V. (1998) *Proc. Natl. Acad. Sci. U. S. A.* **95,** 10547–10552
12. Kholodenko, B. N., and Westerhoff, H. V. (1995) *Biochim. Biophys. Acta* **1229,** 256–274
13. Kholodenko, B. N., and Westerhoff, H. V. (1995) *Trends Biochem. Sci.* **20,** 52–54
14. Hoch, J. A., and Silhavy, T. J., eds. (1995) *Two-component Signal Transduction*, American Society for Microbiology Press, Washington, D. C.
15. Ninfa, A. J. (1996) in *Cellular and Molecular Biology* (Neidhardt, F. C., Curtiss, R., III, Ingraham, J. L., Lin, E. C. C., Low, K. B., Magasanik, B., Reznikoff, W. S., Riley, M., Schaechter, M., and Umbarger, H. E., eds) 2nd Ed., Vol. 1, pp. 1246–1262, American Society for Microbiology, Washington, D. C.
16. Hellingwerf, K. J., Postma, P. W., Tommassen, J., and Westerhoff, H. V. (1995) *FEMS Microbiol. Rev.* **16,** 309–321
17. Briggs, G. E., and Haldane, J. B. S. (1925) *Biochem. J.* **19,** 338–339
18. Cornish-Bowden, A. (1995) *Fundamentals of Enzyme Kinetics*, Portland Press, London
19. Saffen, D. W., Presper, K. A., Doering, T. L., and Roseman, S. (1987) *J. Biol. Chem.* **262,** 16241–16253
20. Scholte, B. J., Schuitema, A. R., and Postma, P. W. (1981) *J. Bacteriol.* **148,** 257–264

21. Mattoo, R. L., and Waygood, E. B. (1983) *Can. J. Biochem. Cell Biol.* **61,** 29–37
22. Waygood, E. B., Meadow, N. D., and Roseman, S. (1979) *Anal. Biochem.* **95,** 293–304
23. Waygood, E. B., Reiche, B., Hengstenberg, W., and Lee, J. S. (1987) *J. Bacteriol.* **169,** 2810–2818
24. Zwaig, N., Kistler, W. S., and Lin, E. C. C. (1970) *J. Bacteriol.* **102,** 753–759
25. Schultz, S. G., and Solomon, A. K. (1961) *J. Gen. Physiol.* **45,** 355–369
26. Winkler, H. H., and Wilson, T. H. (1966) *J. Biol. Chem.* **241,** 2200–2211
27. Bouma, C. L., Meadow, N. D., Stover, E. W., and Roseman, S. (1987) *Proc. Natl. Acad. Sci. U. S. A.* **84,** 930–934
28. Lowry, O. H., Carter, J., Ward, J. B., and Glaser, L. (1971) *J. Biol. Chem.* **246,** 6511–6521
29. Morikawa, M., Izui, K., Taguchi, M., and Katsuki, H. (1980) *J. Biochem.* (*Tokyo*) **87,** 441–449
30. Kodaki, T., Murakami, H., Taguchi, M., Izui, K., and Katsuki, H. (1981) *J. Biochem.* (*Tokyo*) **90,** 1437–1444
31. Rohwer, J. M. (1997) *Interaction of Functional Units in Metabolism: Control and Regulation of the Bacterial Phosphoenolpyruvate-dependent Phosphotransferase System*, Ph.D. thesis, University of Amsterdam
32. Postma, P. W. (1977) *J. Bacteriol.* **129,** 630–639
33. Hogema, B. M., Arents, J. C., Bader, R., Eijkemans, K., Yoshida, H., Takahashi, H., Aiba, H., and Postma, P. W. (1998) *Mol. Microbiol.* **30,** 487–498
34. Zimmerman, S. B., and Trach, S. O. (1991) *J. Mol. Biol.* **222,** 599–620
35. Sauro, H. M. (1993) *Comput. Appl. Biosci.* **9,** 441–450
36. Mendes, P. (1996) in *BioThermoKinetics of the Living Cell* (Westerhoff, H. V., Snoep, J. L., Wijker, J. E., Sluse, F. E., and Kholodenko, B. N., eds) pp. 258–261, BioThermoKinetics Press, Amsterdam
37. Zimmerman, S. B., and Minton, A. P. (1993) *Annu. Rev. Biophys. Biomol. Struct.* **22,** 27–65
38. Garner, M. M., and Burg, M. B. (1994) *Am. J. Physiol.* **266,** C877–C892
39. van Dam, K., van der Vlag, J., Kholodenko, B. N., and Westerhoff, H. V. (1993) *Eur. J. Biochem.* **212,** 791–799
40. Jablonski, E. G., Brand, L., and Roseman, S. (1983) *J. Biol. Chem.* **258,** 9690–9699
41. Stock, J. B., Waygood, E. B., Meadow, N. D., Postma, P. W., and Roseman, S. (1982) *J. Biol. Chem.* **257,** 14543–14552
42. Ruijter, G. J. G., van Meurs, G., Verwey, M. A., Postma, P. W., and van Dam, K. (1992) *J. Bacteriol.* **174,** 2843–2850
43. Waygood, E. B., and Steeves, T. (1980) *Can. J. Biochem.* **58,** 40–48
44. Weigel, N., Kukuruzinska, M. A., Nakazawa, A., Waygood, E. B., and Roseman, S. (1982) *J. Biol. Chem.* **257,** 14477–14491
45. Misset, O., Brouwer, M., and Robillard, G. T. (1980) *Biochemistry* **19,** 883–890
46. Kukuruzinska, M. A., Turner, B. W., Ackers, G. K., and Roseman, S. (1984) *J. Biol. Chem.* **259,** 11679–11681
47. Hoving, H., Koning, J. H., and Robillard, G. T. (1982) *Biochemistry* **21,** 3128–3136
48. Chauvin, F., Brand, L., and Roseman, S. (1994) *J. Biol. Chem.* **269,** 20263–20269
49. Chauvin, F., Brand, L., and Roseman, S. (1994) *J. Biol. Chem.* **269,** 20270–20274
50. Han, M. K., Knutson, J. R., Roseman, S., and Brand, L. (1990) *J. Biol. Chem.* **265,** 1996–2003
51. LiCalsi, C., Crocenzi, T. S., Freire, E., and Roseman, S. (1991) *J. Biol. Chem.* **266,** 19519–19527
52. Waeber, U., Buhr, A., Schunk, T., and Erni, B. (1993) *FEBS Lett.* **324,** 109–112
53. Erni, B. (1986) *Biochemistry* **25,** 305–312
54. Rohwer, J. M., Hofmeyr, J.-H. S., and Postma, P. W. (1998) in *BioThermoKinetics in the Post Genomic Era* (Larsson, C., Påhlman, I.-L., and Gustafsson, L., eds) pp. 340–344, Göteborg University, Göteborg, Sweden
55. Feese, M., Pettigrew, D. W., Meadow, N. D., Roseman, S., and Remington, S. J. (1994) *Proc. Natl. Acad. Sci. U. S. A.* **91,** 3544–3548
56. Misset, O., Blaauw, M., Postma, P. W., and Robillard, G. T. (1983) *Biochemistry* **22,** 6163–6170
57. Minton, A. P. (1983) *Mol. Cell. Biochem.* **55,** 119–140
58. Rohwer, J. M., Bader, R., Westerhoff, H. V., and Postma, P. W. (1998) *Mol. Microbiol.* **29,** 641–652
59. Plumbridge, J. (1999) *Mol. Microbiol.* **33,** 260–273
60. Maeda, T., Wurgler-Murphy, S. M., and Saito, H. (1994) *Nature* **369,** 242–245
61. Moe, G. R., Bollag, G. E., and Koshland, D. E., Jr. (1989) *Proc. Natl. Acad. Sci. U. S. A.* **86,** 5683–5687
62. Kholodenko, B. N., Molenaar, D., Schuster, S., Heinrich, R., and Westerhoff, H. V. (1995) *Biophys. Chem.* **56,** 215–226
63. Schuster, S., and Heinrich, R. (1992) *BioSystems* **27,** 1–15
64. Lolkema, J. S. (1995) *Biochim. Biophys. Acta* **1252,** 284–294
65. Weigel, N., Waygood, E. B., Kukuruzinska, M. A., Nakazawa, A., and Roseman, S. (1982) *J. Biol. Chem.* **257,** 14461–14469
66. Saier, M. H., Jr., Schmidt, M. R., and Lin, P. (1980) *J. Biol. Chem.* **255,** 8579–8584
67. Beneski, D. A., Nakazawa, A., Weigel, N., Hartman, P. E., and Roseman, S. (1982) *J. Biol. Chem.* **257,** 14492–14498
68. Anderson, J. W., Bhanot, P., Georges, F., Klevit, R. E., and Waygood, E. B. (1991) *Biochemistry* **30,** 9601–9607
69. Reizer, J., Sutrina, S. L., Wu, L.-W., Deutscher, J., Reddy, P., and Saier, M. H., Jr. (1992) *J. Biol. Chem.* **267,** 9158–9169
70. Meadow, N. D., and Roseman, S. (1982) *J. Biol. Chem.* **257,** 14526–14537
71. Vogler, A. P., Broekhuizen, C. P., Schuitema, A., Lengeler, J. W., and Postma, P. W. (1988) *Mol. Microbiol.* **2,** 719–726
72. van der Vlag, J., and Postma, P. W. (1995) *Mol. Gen. Genet.* **248,** 236–241
73. Grenier, F. C., Waygood, E. B., and Saier, M. H., Jr. (1986) *J. Cell. Biochem.* **31,** 97–105